

# Models for the Prediction of Performance and Emissions in a Spark Ignition Engine - A Sequentially Structured Approach

Ivan Arsie, Cesare Pianese, Gianfranco Rizzo

Department of Mechanical Engineering, University of Salerno, Italy

Copyright © 1998 Society of Automotive Engineers, Inc.

## ABSTRACT

A thermodynamic model for the simulation of performance and emissions in a spark ignition engine is presented. The model is part of an integrated system of models with a hierarchical structure developed for the study and the optimal design of engine control strategies. In order to reduce the uncertainty due to the mutual interference during the validation phase, the model has been developed accordingly with a hierarchical and sequential structure.

The main thermodynamic model is based on the classical two zone approach. A multi-zone model is then derived from the two zone calculation, for a proper evaluation of temperature gradients in the burned gas region. The emissions of HC, CO and NO<sub>x</sub> are then predicted by three sub-models.

In order to make the precision of emission models suitable for engine control design, an identification technique based on decomposition approach has been developed, for the definition of optimal model structure with a minimum number of parameters.

The results of the thermodynamic cycle model validation, performed over more than 300 engine operating conditions, show a satisfactory level of agreement between measured and predicted data cycles. Afterward, the two step identification procedure has been applied for the emission models parameters identification. From this analysis, it has been found that the model precision achieved can be comparable with that obtained via conventional mapping procedures using black-box models, but with a drastic reduction of the experimental effort. Moreover, the proposed approach allows substantial computational time saving with respect to conventional identification techniques.

## INTRODUCTION

Many models for the study and the design of internal combustion engines (ICE's) have been proposed in literature, in order to assist the development of engines with performance complying with future pollution control regulations. Much effort is being spent toward the

development of comprehensive 3-D models, describing all the relevant phenomena relating to engine operation and emission formation at the maximum allowed level of detail. Although their use can be precious in order to consider the mutual influence of geometrical and operating parameters on the complex fluid-dynamics and thermo-chemical phenomena involved in engine operation, they do not yet represent the ultimate solution for all applications in the ICE's sector. The practical utility of these models, which require very high computational power, may be questionable in those cases where many repeated computations are involved, as in design applications. Moreover, their quantitative precision, which requires an appropriate "balanced precision" in all their sub-models, could even be inadequate for some applications.

Therefore, notwithstanding the continuous effort toward the development of comprehensive 3-D models, many different models can still be found in literature, often characterized by substantial differences in structure, goals and complexity [1], [4], [5], [9]. A significant number of them are devoted to design of optimal engine control strategies and to the development of new engine control technologies. They range from input-output black-box models, mostly oriented to control design, to gray-box mean-value models, with a simplified description of the most relevant physical processes [1],[2],[3], up to complex 3-D fluid-dynamic models [4],[5]. These classes of model substantially differ in terms of computational time and experimental data required: for the validation of the simplest black-box models, hundreds or thousands of engine data could be needed to compensate for the lack of physical information, resulting in high experimental effort and lower model flexibility; on the other hands, the computational cost of the detailed 3-D models is not compatible with many control applications.

## THE MODELING APPROACH

From these considerations, it emerges that in many cases a proper solution could be represented by the adoption of a suitable mixed approach, in order to combine the advantages of various kind of models.

A hierarchical model structure (figure 1) has been developed by the authors for the optimal design of engine control strategies [6], where it is assumed that the engine geometry is assigned. At the final stage, this set of models will be embedded in a more general engine control strategy rapid prototyping procedure. A gray-box mean-value dynamical model [8],[9] is linked with the computer code ODECS for control simulation and optimization [10], which is now in use by Magneti Marelli. At higher level, phenomenological models [11] are used in conjunction with experimental techniques to simulate in off-line mode engine performance to build fast black-box model, which in turn are used for optimal design of engine control strategies [6], [11], [24]. The interaction between experiments and models can be superintended by interactive Experimental Design techniques, which can give further substantial benefits in guiding and reducing the experimental tests needed for engine model validation [7].

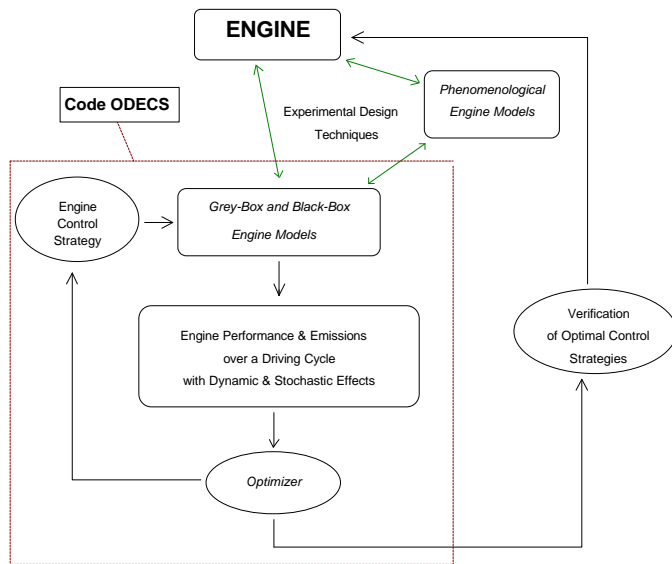


figure 1 – A hierarchical model structure for engine control design

The phenomenological models have been built according to a sequential structure of modules, rather than as a single comprehensive block. This approach offers a substantial advantage in the validation phase, because it is possible to identify the values of the model parameters just acting on the appropriate module, and limiting the uncertainty due to mutual influences and correlation among the variables.

The adoption of a suitable sequential structure and of identification techniques based on decomposition approach has allowed substantial saving of computational power with respect to conventional approaches in determining structure and values of the model parameters for engine emissions [12], whose knowledge represents an important task for control applications. At this moment, fully predictive emission models suitable for the optimal design of engine control strategies, which requires extensive computations, are not yet available. Therefore, some model parameters

must be identified by comparison with experimental data, and their relationships with operating variables determined, in order to use the model for prediction. To this purpose a parameter identification procedure based on decomposition approach has been proposed in order to reduce the number of engine experimental data and the computational time required for model validation [12].

In the following chapters, the main features of the thermodynamic engine model used in the above described hierarchical structure are presented, and a set of results for emission prediction levels reviewed. Afterward, the results obtained by the use of the decomposition approach for the identification of emission model parameters are presented and discussed.

## THE THERMODYNAMIC MODEL

The prediction of emission levels requires an accurate description of thermodynamic, fluid dynamic and chemical processes occurring inside the combustion chamber. Moreover, for the three main engine exhaust products (HC, CO, NO<sub>x</sub>), the formation processes are characterized by different mechanisms which must be described with suitable independent sub-models. The approach followed in the present work is based on a two zone model [13] to predict in-chamber pressure and burned and unburned gas temperature as function of engine geometry and operating parameters. Then, starting from the two-zone calculation, three different sub-models are used for the simulation of each emission product.

## TWO ZONE THERMODYNAMIC MODEL

The classical approach described by Ferguson [13] has been selected for the thermodynamic simulation of S.I. engine due to its simple formulation, for the well structured documentation available and for its high computational efficiency. The model is briefly reviewed in the following.

The combustion chamber is divided into two zones, corresponding to burned and unburned gas regions, by an infinitesimal flame front with a spherical shape. In each zone the thermodynamic state is defined by the mean thermodynamic properties; the burned gas are assumed in chemical equilibrium during combustion and for the main expansion stroke, while near the end of the expansion process the mixture is assumed frozen [4],[5],[13],[14].

To account for the radial evolution of flame front a burned mass fraction function  $x$  is used to describe the spatial dynamics of combustion process. Assuming  $m$  the total mass evolving in the cylinder, the specific internal energy is:

$$u = \frac{U}{m} = xu_b + (1-x)u_u \quad (1.)$$

where subscripts  $u$  and  $b$  refer to unburned and burned gas respectively.  $u_u$  is the specific internal energy of unburned gases at temperature  $T_u$  and  $u_b$  is the specific internal energy of burned gases at temperature  $T_b$ . An analogous relation is derived for the specific volume:

$$v = \frac{V}{m} = xv_b + (1-x)v_u \quad (2.)$$

The energy balance for an open system bounded by combustion chamber walls holds [13]:

$$m \frac{du}{dq} + u \frac{dm}{dq} = \frac{dQ}{dq} - P \frac{dV}{dq} - \frac{\dot{m}_l h_l}{w} \quad (3.)$$

where  $q$  is crank angle,  $w$  angular speed,  $m$  total mass in the cylinder,  $u$  specific internal energy (eq. 1),  $Q$  amount of heat flowing into the control volume,  $P$  gas pressure and  $V$  total volume. The last term in equation (3) represents the energy flow due to blow-by. The heat flow model describes heat transfer between gas and cylinder walls:

$$\frac{dQ}{dq} = \frac{-\dot{Q}_l}{w} = \frac{-\dot{Q}_b - \dot{Q}_u}{w} \quad (4.)$$

In the above equation the two heat flux terms for burned and unburned gases are modeled as follows:

$$\dot{Q}_b = \mathbf{h}_b A_b (T_b - T_w) \quad (5.)$$

$$\dot{Q}_u = \mathbf{h}_u A_u (T_u - T_w) \quad (6.)$$

where  $A_b$  and  $A_u$  are the combustion chamber wall areas in contact with burned and unburned gases respectively and  $T_w$  is the cylinder wall temperature. The surface areas are computed as function of cylinder bore  $b$  and instantaneous combustion chamber volume  $V$  with the following relations:

$$A_b = \left( \frac{pb^2}{2} + \frac{4V}{b} \right) x^{1/2} \quad (7.)$$

$$A_u = \left( \frac{pb^2}{2} + \frac{4V}{b} \right) (1-x)^{1/2} \quad (8.)$$

It is assumed that the burned gas contact wall surface is proportional to the square root of burned mass fraction to account for the greater volume filled by burned gases with respect to unburned ones. These relationships are consistent with the whole heat exchange model described below.

The instantaneous convective heat transfer coefficient  $\mathbf{h}$

[W/m<sup>2</sup>/K] is computed from the well known correlation proposed by Woschni [14] as function of cylinder bore  $b$  [cm], pressure  $P$  [bar], gas temperature  $T$  [K] and mean gas velocity  $w$  [m/s]:

$$\mathbf{h} = 326 \cdot b^{-0.2} \cdot P^{0.8} \cdot T^{-0.55} \cdot w^{0.8} \quad (9.)$$

with the mean gas velocity  $w$  related to the mean piston speed  $\overline{U}_p$  and combustion phenomena [4],[13]:

$$w = \left[ C_1 \overline{U}_p + C_2 \frac{VT_0}{P_0 V_0} (P - p_m) \right] \quad (10.)$$

$T_0$ ,  $P_0$  and  $V_0$  are temperature, pressure and volume at inlet valve closing, respectively;  $p_m$  is the motored pressure. The constants  $C_1$  and  $C_2$  are derived from Woschni [14].

Thermodynamic gas properties routines have been implemented from Ferguson [13] and adapted to the purpose of the present work. These routines give the thermodynamic gas properties as function of pressure, temperature and equivalence ratio  $f$  for the mixture of air, fuel and residual gas fraction  $f$  (FARG) and for the mixture of burned gases at equilibrium (ECP):

$$(u, v, h, \frac{q}{T_b}, \frac{q}{p}) = f(T_b, p, f) \quad (11.)$$

$$(u, v, h, \frac{q}{T_u}, \frac{q}{p}) = f(T_u, p, f, f) \quad (12.)$$

For the heat release law the well suited Wiebe function has been applied [4] to compute the burned mass fraction  $x(q)$ :

$$x = \begin{cases} 0 & q < q_s \\ 1 - \exp \left[ \ln(0.001) \cdot \left( \frac{q - q_s}{q_b} \right)^n \right] & q > q_s \end{cases} \quad (13.)$$

where  $q_s$  is the ignition crank angle and  $q_b$  the combustion angular period. In accordance with Heywood [4] the parameter  $n$  has been fixed to a constant value of 3.

The problem described with equation (1) through equation (10), relating the in-cylinder pressure variation rate, the amount of work and heat exchange as function of crank angle, constitutes a set of ordinary differential equations. For the integration of this system a 4th order Runge-Kutta scheme with adaptive step size has been adopted [15].

## EMISSIONS MODELS

From the thermodynamic model just described, the burned mass fraction, the pressure and the mean

temperatures are computed for each crank angle, together with other useful data relating to work, heat transfer and chemical equilibrium properties of burned and unburned gases. Starting from the two zone engine cycle simulation, the emissions levels for HC, CO and NO<sub>x</sub> are predicted through three distinct sub-models.

The NO<sub>x</sub> and CO formation is controlled by chemical kinetic reactions [4],[5],[16],[17], therefore their production rates are non-linearly dependent from burned gas temperature. Thus, the two-zone model approximation is not feasible to account for different thermo-chemical states experienced by burned gas regions throughout the combustion process until the end of expansion stroke. Therefore, a multi-zone discretization of burned gas region has been considered following the approach described in the next section.

The mechanisms which mainly influence the HC emissions are the adsorption and desorption of unburned hydrocarbons into the wall wetting oil layer, the inflow and outflow from the crevices and the post-flame oxidation [18],[19], while experimental evidences [20] show that the flame quenching on the walls is not a predominant formation mechanism. Moreover, the diffusion of hydrocarbons from the quenching layer into the bulk gas takes places in few milliseconds resulting in a limited amount of unburned hydrocarbons left on the wall surfaces [4].

#### MULTI-ZONE THERMAL MODEL

To account for different gas composition and temperature gradients occurring in the various combustion chamber regions (e.g. spark plug, piston head), the burned gas volume is divided into  $N^*$  zones representing an adiabatic core region. A further external zone has been also considered as thermal boundary region of the central adiabatic core zones, primarily responsible for the heat transfer. It is assumed that no mixing occurs between neighboring zones and that at the end of combustion the same mass fraction is present in each zone (see figure 2). This schematization is consistent with the hypothesis that burned gases experience a continuous adiabatic compression process as the combustion proceeds [4],[5],[21].

From the ignition event the formation of the first zone starts, the development of this region ending when the first  $1/N^*$ -th mass fraction has burned. Afterward a new region formation begins and the process goes on until a further  $1/N^*$  amount of mass has burned. The formation of the other zones proceeds analogously until the end of combustion, where the total amount of burned gas is distributed among the boundary layer and the  $N^*$  zones. Since the zones are formed from the latest burned gases and the flame front is assumed spherical, the actual forming region is the most external one and is adjacent to the flame front.

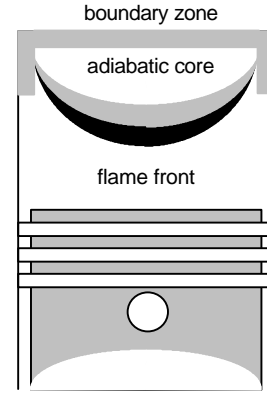


figure 2 - Combustion chamber with multi-zone schematization.

The mass of boundary layer is computed as a product of its volume and density. The volume is derived from geometrical considerations assuming a constant thickness, while the density is derived from a logarithmic weighted average between wall and mean burned gas temperatures.

The current temperature of the already formed zones is computed accordingly with an adiabatic isentropic compression, which for the  $j$ -th zone at current crank angle  $q_i$  can be written as follows [5], [21]:

$$T_j(q_i) = T_j(q_{i-1}) \left( \frac{P(q_i)}{P(q_{i-1})} \right)^{\frac{g-1}{g}} \quad (14.)$$

To derive both burning mass and the temperature of the zone adjacent to the flame front (i.e. forming zone) an energy-mass balance equations system is written. The energy balance between the boundary layer, the formed zones and the burning zone compared with the mean burned gas energy, computed with the two zones model is assumed. The mass balance is related with the distribution of the last burned gas fraction among the boundary layer and the flame front where the adiabatic flame temperature is considered.

The resulting burned gas temperature distribution will therefore depend on the parameters describing the thermal boundary layer and on the assumed number of zones in burned gas, which can account for the relative role of mixing processes and heat transfer.

#### CARBON MONOXIDE FORMATION MODEL

From experimental evidence the CO levels at exhaust of internal combustion engines are mainly related with mixture equivalence ratio. Nevertheless, the exhausted CO concentrations are lower than in-chamber measured CO while higher concentrations are found in comparison with CO equilibrium concentration at exhaust reference conditions [4]. These considerations allow the assumption of a chemical kinetically controlled CO formation process [5], which in turn requires a detailed

description of burned gases thermal field being modeled with the previous multi-zone model.

The formation and decomposition of carbon oxide is mainly controlled by the following chemical reactions:



though the latter influence is remarkable only for high temperatures.

Assuming that OH, CO<sub>2</sub> and O<sub>2</sub> are in chemical equilibrium state, the CO concentration rate of variation is:

$$\frac{1}{V_b} \frac{dn_{CO}}{dt} = (R_1 + R_2) \cdot \left( 1 - \frac{[CO]}{[CO]_e} \right) \quad (17.)$$

where  $n_{CO}$  is the number of moles present in the burned gas volume  $V_b$ , while the equations equilibrium rates are given by:

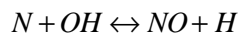
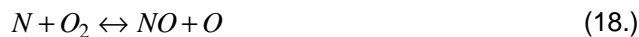
$$R_1 = k_1^+ [CO]_e [OH]_e \quad k_1^+ = 6.76 \cdot 10^{10} \cdot \exp\left(\frac{T}{1102}\right)$$

$$R_2 = k_2^- [CO]_e [O_2]_e \quad k_2^- = 2.5 \cdot 10^{12} \cdot \exp\left(\frac{-24055}{T}\right)$$

The equation (17) is solved numerically with a fourth order Runge-Kutta scheme for each of  $N^*$  zones, and the final CO concentration is computed as the volume weighted mean of CO concentration for each zone.

## NITROGEN OXIDES FORMATION MODEL

To describe the NO formation process the extended Zeldovich mechanism is adopted [4],[5],[16],[17]:



Some simplification can be made to the above system of reactions. Due to the low concentration level of atomic nitrogen, a steady state assumption is made:

$$\frac{d[N]}{dt} \approx 0 \quad (19.)$$

Moreover, since the energy contribution of NO reactions to the combustion process energy balance is negligible and due to their high energy activation levels, the decoupling of the NO formation mechanism from the main combustion chemical kinetics reactions, which in turn exhibit higher reaction rates, is assumed. Thus, in

the reactions set (18) is useful to consider the equilibrium concentration for O, O<sub>2</sub>, OH, H and N<sub>2</sub> in the completely burned gas zones.

Once these assumptions are made, the Zeldovich mechanism holds the following rate of variation for the moles of NO [21]:

$$\frac{1}{V_b} \frac{dn_{NO}}{dt} = \frac{2R_1 \left\{ 1 - \left( \frac{[NO]}{[NO]_{eq}} \right)^2 \right\}}{1 + \left( \frac{[NO]}{[NO]_{eq}} \right) \frac{R_1}{R_{2+} + R_3}} \quad (20.)$$

where  $n_{NO}$  is the number of moles present in the burned gas volume  $V_b$ , while  $R_1$ ,  $R_2$  and  $R_3$  are computed as follows:

$$R_1 = k_1^+ [O]_e [N_2]_e \quad k_1^+ = 7.6 \cdot 10^{13} \cdot \exp\left(\frac{-38000}{T}\right)$$

$$R_2 = k_2^- [NO]_e [O]_e \quad k_2^- = 1.5 \cdot 10^9 \cdot \exp\left(\frac{-19500}{T}\right)$$

$$R_3 = k_3^- [NO]_e [H]_e \quad k_3^- = 2 \cdot 10^{14} \cdot \exp\left(\frac{-23650}{T}\right)$$

The relationships reported for the reaction rate constants  $k_1$ ,  $k_2$  and  $k_3$  are the most frequently used in the literature [4],[21]; such values present some uncertainty due to the experimental tests they have been carried out with. The exhausted gas NO<sub>x</sub> concentration is a volume weighted mean of the NO<sub>x</sub> concentration computed for each zone.

At moment in this sub-model the formation of prompt NO, which is formed in the flame reaction zone, is neglected. It has been shown [4] that the NO produced in the post-flame region is the main source of S.I. engine exhausted NO; nevertheless, some improvements in the model will be carried out to account for prompt NO also.

## UNBURNED HYDROCARBONS

After Schramm and Sorenson [18] the HC formation mechanism can be briefly summarized in the following points:

- the unburned mixture fills the piston crevices during compression stroke and is released during expansion; the mixture released ahead the flame front is burned instantaneously, while the mixture released in the burned region undergoes a kinetically controlled oxidation process;
- the oil film layer adsorbs the mixture fuel during intake and compression strokes, part of this fuel is

desorbed behind the flame front and is oxidized following the same oxidation process cited in the above point.

The mass mixture rate of change in the crevices is:

$$\frac{dm_{cr}}{dq} = \frac{dP(q)}{dq} \frac{RT_p}{V_{cr}} \quad (21.)$$

where  $m_{cr}$  is the mixture mass in the crevices volume  $V_{cr}$ ,  $P$  is the in-cylinder pressure and  $T_p$  the piston temperature.

The adsorption/desorption of fuel into the oil layer is modeled with the following one-dimensional Fourier equation expressing the fuel mass concentration rate of change in the oil film:

$$\frac{\partial Y}{\partial t} = D \frac{\partial^2 Y}{\partial x^2} \quad (22.)$$

where  $Y$  is the fuel mass concentration in the oil,  $D$  ( $1.6 \cdot 10^{-5}$  [cm<sup>2</sup>/sec], [19]) is the diffusion coefficient for the fuel in the oil and  $x$  is the radial coordinate of oil film. This partial differential equation is solved with a finite difference explicit scheme where the space derivative is approximated with a second order central formula, while time integration is performed with a fourth order Runge-Kutta method. The oil film layer domain has been discretized in space with 20 slices, with radial symmetry each, and 10 concentric computational cells. From Schramm and Sorenson [18] and Trinker et al. [19], for space boundary conditions von Neumann condition at cylinder wall (i.e. zero gradient of fuel concentration) is chosen. At oil film-gas interface the current concentration is derived from Henry's law which relates the fuel mole fraction in the oil as function of the fuel gas phase partial pressure in the mixture through the Henry's constant (1.069 [atm], [19]). For a more detailed description of Henry's law the reader is addressed to the references [18], [19]. As initial conditions it is assumed that no fuel is present in the oil film.

The fuel released into the burned gas region is oxidized in a boundary layer near the wall with an intermediate temperature derived from wall and mean burned gas temperatures. This post-flame oxidation is governed by the following Arrhenius equation [18]:

$$\frac{d[HC]}{dt} = -C_R k_1 [HC][O_2] \exp\left(-\frac{37230}{RT}\right) \quad (23.)$$

where the kinetic rate  $k_1$  is equal to  $7.7 \cdot 10^{15}$ , while  $C_R$  is a calibration constant which is used to fit the experimental data with the model parameter identification described in the next section.

In the present model the HC post-flame oxidation is

supposed to end at the exhaust opening valve crank angle, while in the real engine the HC oxidation continues during the exhaust stroke into the exhaust manifold. This further process will be considered in the future version of the whole model which will take into account the intake and exhaust strokes. After the implementation of exhaust valve flow sub-model the implementation of post-flame oxidation in the exhaust port will be a straightforward task. As shown in the results section, neglecting this additional oxidation process the final HC concentration simulated will be overestimated with respect the measured concentration.

## MODEL PARAMETER IDENTIFICATION

From the description of the thermodynamic model presented, it emerges that some model parameters should be identified in order to make the model suitable for prediction.

The main unknown parameters of the presented model are the variables which affect the heat release law (combustion time duration  $t_b$  and the Wiebe exponent coefficient  $n$ ), the heat transfer parameters and the further parameters which influence temperature stratification and emission formation.

An effective identification of all unknown model parameters could not be achieved by conventional techniques, due to the strong non linearities of the model and to the correlation existing between some set of parameters (e.g. between combustion duration and Wiebe exponent  $n$ , heat transfer coefficient and combustion chamber wall temperature). The uncertainty due to the combined effect of these mutual correlations and of the measurement errors would not allow in practical cases a precise parameter identification. Therefore, a sequential identification procedure has been adopted.

## HEAT TRANSFER

An estimation of mean cylinder wall temperature (see eqs. 5 and 6) is made by processing measured pressure data during compression stroke. This temperature is assumed equal to the temperature of the gas at the crank angle where the instantaneous polytropic compression exponent is equal to the corresponding adiabatic iso-entropic one. Heat transfer coefficients can be then estimated by least square techniques. This approach allow to overcome the quoted problems due to the mutual correlation of wall temperature with heat transfer coefficients [23].

## COMBUSTION MODEL

Combustion time values have been identified by least square techniques [11], whereas for Wiebe exponent a constant value is used. Other parameters exerting secondary influence on cycle prediction are taken from literature data. For each pressure cycle the combustion time duration  $t_b$  is identified by means of non linear least

squares through direct comparison of measured and predicted pressure cycles [15], [22], by use of minimization algorithms:

$$\min_{t_b} STDV(t_b) = \sqrt{\frac{\sum_{i=q_{IVC}}^{q_{EVO}} [p_{meas}(q_i) - p_{sim}(q_i, t_b)]^2}{q_{EVO} - q_{IVC}}} \quad (24.)$$

In order to determine a correlation to be used in the thermodynamic model for prediction application, the following regression has been derived from physical consideration on laminar flame velocity [5]:

$$t_b = \frac{a_1 [rpm^{a_6} f^{a_7} (a_8 + \exp(a_9 q_s)) \dot{m}_a^{a_{10}}]}{\left(\frac{T_s}{298}\right)^{(a_2 + a_3 a)} p_s^{(a_4 + a_5 a)}} \quad (25.)$$

where  $a$  is the air-fuel ratio,  $T_s$  and  $p_s$  are the in-cylinder temperature and pressure at spark advance angle  $q_s$ ,  $f$  is the residual mass fraction and  $\dot{m}_a$  is the air mass flow rate.

## EMISSION MODELS

For the parameters identification of the emission models, a procedure based on the decomposition approach has been proposed.

A general non-linear "physical" model (subscript ph) expresses the output variable  $y$  (i.e. HC, CO or NOx emissions) as function of engine operating variables  $n$  and of a vector of parameters  $p$ :

$$y_{ph,i} = f(p_i, n_i) \quad (26.)$$

where subscript  $i$  refers to given engine operating conditions. The parameters  $p$  can represent physical quantities used in the model, as kinetic rates, number of zones to account for temperature stratification in burned gases, various coefficients. In general, their values could not be considered constant over the entire operational range of the engine. Therefore, they can be in turn expressed as a function of the engine operating variables  $n$ , by means of  $N$  further parameters  $b$ , in order that the model could be used in a predictive way over the whole operational range:

$$y_{ph,i} = f(p_i(b, v_i), n_i, b) \quad (27.)$$

A direct approach would require the following steps:

- i) specification of the parameters  $p$  of the physical model;
- ii) specification of functional structure of the relationships  $p(b, n)$ ;
- iii) determination of the optimal values of the  $N$  parameters  $b$  by comparison of computed and

observed values over the set of  $M$  experimental conditions, solving a non linear regression problem:

$$\min_b S(b) = \sum_{i=1}^M \left( y_i(p_i(b, v_i), n_i, b) - y_i^* \right)^2 \quad (28.)$$

- iv) estimation of statistical significance of the solution.

It can be observed that step iii) involves repeated model evaluation over the entire set of experimental data. For real cases, (i.e.  $N=10-50$ ,  $M \approx 300$ ), many thousands of model evaluations would be therefore required, with very high computational cost. Moreover, the entire process from ii) to iv) should be repeated each time that a different functional structure  $p(b, n)$  has to be assumed.

In order to overcome these problems, a two-phases decomposition approach is proposed.

The first phase would require the following steps:

- a) specification of the parameters  $p$  of the physical model;
- b) determination of an intermediate model  $y_i(p)$  (i.e. 2nd order Taylor approximation) to describe the influence of the physical parameters  $p$  which exert a non linear influence on the model:

$$y_{i,i}(p) = y_{ph}(p_0) + \sum_{j=1}^N (p_j - p_{0j}) \frac{\partial y_{ph}}{\partial p_j} + \frac{1}{2} \sum_{k=1}^N \sum_{j=1}^N (p_j - p_{0j}) (p_k - p_{0k}) \frac{\partial^2 y_{ph}}{\partial p_j \partial p_k} \quad (29.)$$

- c) for each  $i$ -th operating condition, numerical computation of gradient and Hessian, and their storage in data files;
- d) evaluation of the approximation errors  $e_{i,j}$  for finite variations of each parameter around its nominal value  $p_{0,j}$ :

$$e_{i,j} = y_i^* - y_{ph,i}(p_{0,1}, \dots, p_{0,j-1}, k p_{0,j}, p_{0,j+1}, \dots, p_{0,N}) \quad (30.)$$

with  $k = 1.1$  if a 10% variation is applied.

The total approximation error  $e_i$  can then be estimated by a linear model:

$$e_i = \frac{1}{x} \sum_{j=1}^P e_{i,j} \frac{p_j - p_{0,j}}{p_{0,j}} \quad (31.)$$

The second phase is composed of the following steps:

- e) specification of a functional structure  $p(b, n)$ ; the following general polynomial relationship has been used:

$$p_{i,k} = \sum_{j=1}^N c_{j,k} b_j \prod_{l=1}^L n_{i,l}^{f_{j,k,l}} \quad (32.)$$

where the actual functional form is determined by the matrices  $\phi$  and  $\chi$ ; this latter assumes 0 or 1 values, and can be changed according to the stepwise procedure to include or exclude some terms in eq. (32);

- f) determination of the optimal values of the parameters  $\beta$  by solving a non linear constrained minimization problem (33, 34), using the Taylor approximation; constraints (34) are introduced to avoid that unfeasible solutions could be proposed, where the estimated approximation error is larger than a given limit  $e_{\max}$ :

$$\min_b S(b) = \sum_{i=1}^M \left( y_i(p_i(b, v_i), \rho_i, b) - y_i^* \right)^2 \quad (33.)$$

$$e_i(b) \leq e_{\max} \quad i = 1, M \quad (34.)$$

the optimization problem has been solved by Augmented Lagrangian approach, using the Powell conjugate directions algorithm [15] [22];

- g) estimation of the limits of confidence regions at level of probability  $(1-a)$  for parameters  $b$ , by numerical solution of the following equation:

$$S(b) = S(b^*) \left[ 1 + \frac{N}{M-N} F(N, M-N, 1-a) \right] \quad (35.)$$

where  $S(b^*)$  represents the sum of squares corresponding to the solution of problem (33, 34), and  $F$  is the Fisher distribution with  $N$  parameters,  $M$  observations at  $(1-a)$  probability [25];

- h) elimination of the less significant parameters  $\beta$ , by zeroing the corresponding  $\chi$  values in eq. (32);  
i) check of the termination criteria and repetition of steps f and g (backward stepwise regression).

This procedure offers the following advantages:

- Only the first phase requires a full model evaluation on the entire data set (step c) to compute gradient and Hessian. This information can be stored and easily updated if further parameters would be added to the model. Parallel or concurrent computational techniques can also be easily used in such phase.
- Each iteration of the regression technique (step f) is much more faster since it operates on polynomial approximations rather than on the full model.
- The resulting objective function is quadratic, with linear constraints, and very fast convergence can be achieved by classical optimization techniques.
- The entire process can be easily iterated for each different model parametrization, and a stepwise approach can be followed in order to determine the most significant model parameters.
- As final result, an entire class of models with a decreasing number of parameters is obtained, and a trade-off between number of parameters and fitting

precision can be achieved.

## RESULTS

In the following, the result of the combustion time duration identification together with the prediction of emission levels are reported, in comparison with experimental data. The purpose of this analysis is to verify the physical correctness and the precision of each emission submodels in order to define a starting accuracy level before the use of the two step identification procedure summarized at the end of the previous section. To show the precision improvement achievable with the decomposition approach some results are also presented.

The thermodynamic model has been validated over a large set of experimental data; 342 engine pressure cycles have been measured on FIAT 2 liters S.I. engine on a dynamic test bench at CNR - Istituto Motori and are representative of engine working operation for an ECE 15 transient cycle.

In the figure 3 the rms between predicted and measured pressure cycles distribution is reported after the identification of combustion time duration. As it can be seen from the figure most of simulated cycles exhibit an error less then 0.5 [bar], which expresses a satisfactory level of precision achievable with the thermodynamic model.

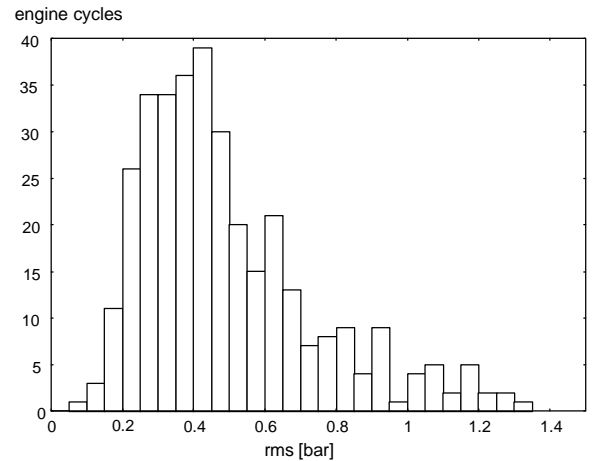


figure 3 - Rms of computed and measured pressure cycle distribution for 342 engine cycles.

A non linear parameter identification has been performed to find the ten coefficients  $a_i$  of equation (25). The comparison between identified combustion time and the data simulated through the equation (25) are shown in the figure 4, where a satisfactory prediction level for equation (25) is evidenced; the correlation index for the identification parameters analysis is  $R^2 = 0.88$ .

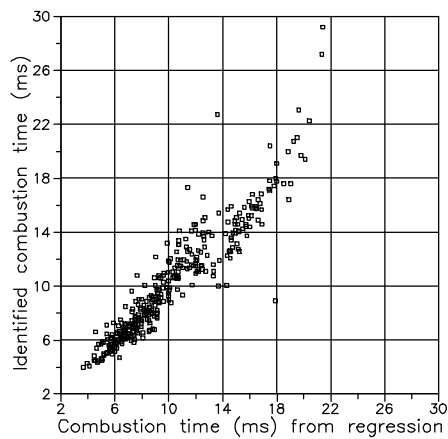


figure 4 - Comparison between identified and simulated (eq. 25) combustion time duration.

Starting from the engine cycle simulation, performed using the burning time identified, the emissions levels have been predicted with the three sub-models before described. The computations refer to the 342 engine working conditions investigated during the experimental analysis. Regard to the emission sub-models, the presented results have been obtained with standard values of the parameters, taken from literature data (e.g. kinetic constants, film layer thickness, volume crevices, number of zones). These results represent the starting point for the identification of the emission models [12].

In the figure 5 the results of CO predictions are compared with the measured exhaust port CO levels; as it was expected, the maximum uncertainty in the simulations is found in the region of low CO emission levels around lean operating points. To show the ability of the sub-model in capturing the main physical features of CO formation process, the comparison of predicted and measured CO levels as function of air-fuel ratio for two engine operating condition is presented in figure 6 and figure 7.

For the  $\text{NO}_x$  the comparison of predicted emission levels with experimental data is reported in the figure 8. The analysis of the figure evidences the scattering of computed data set; nevertheless in the mean the prediction can be considered acceptable since neither underestimation or overestimation are found. Besides, the capability of the sub-models in describing the physical influence of the engine operating conditions on the  $\text{NO}_x$  formation process is displayed in the figure 9 and figure 10 where predicted and measured  $\text{NO}_x$  levels as function of air-fuel ratio are plotted.

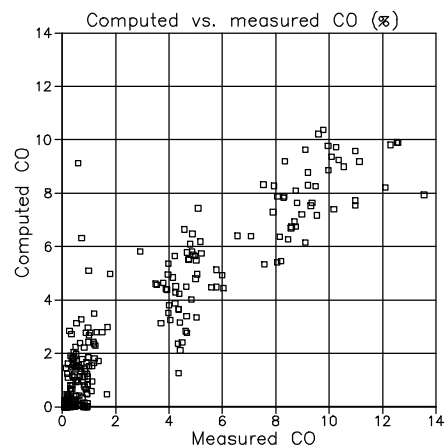


figure 5 - Computed vs. measured CO -  $R^2=0.858$ .

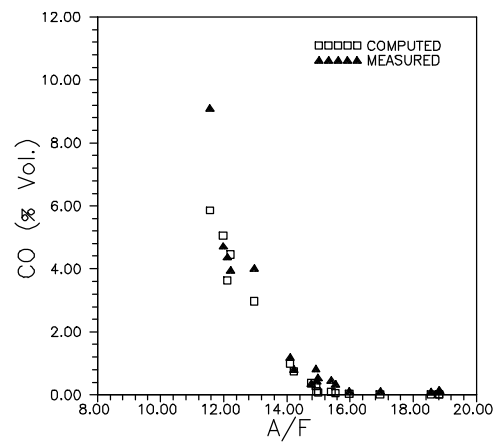


figure 6 - Comparison between computed and measured CO as function of Air-Fuel ratio at 2000 rpm, 50 [Nm] Torque.

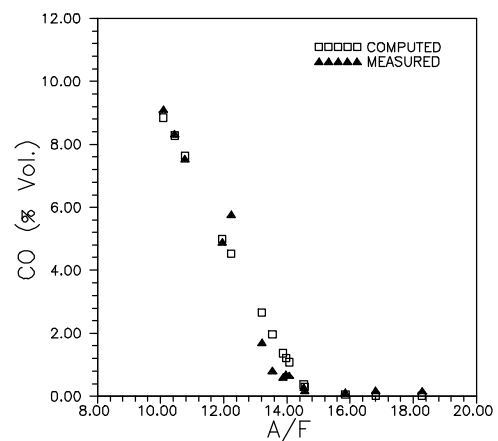


figure 7 - Comparison between computed and measured CO as function of Air-Fuel ratio at 3000 rpm, 90 [Nm] Torque.

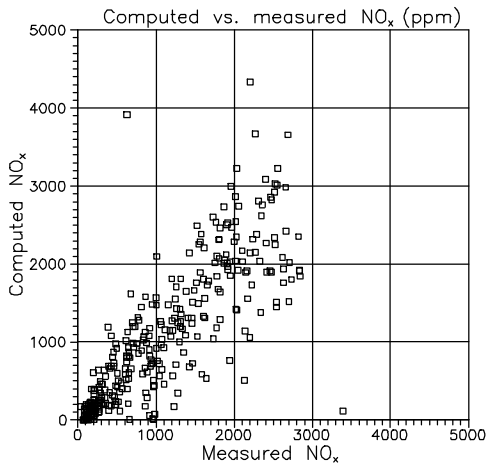


figure 8 - Computed vs. measured  $\text{NO}_x$  -  $R^2=0.449$ .

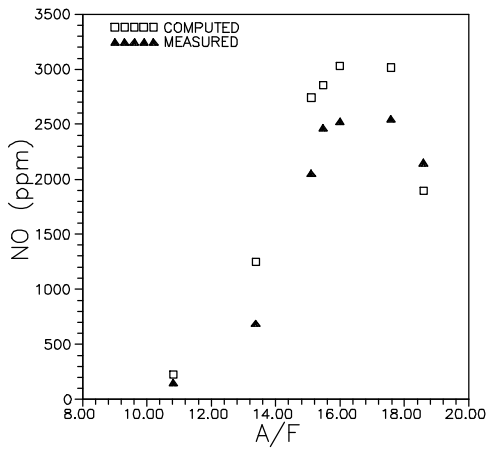


figure 9 - Comparison between computed and measured  $\text{NO}_x$  as function of Air-Fuel ratio at 1000 rpm, 30 [Nm] Torque and spark advance 35 [deg].

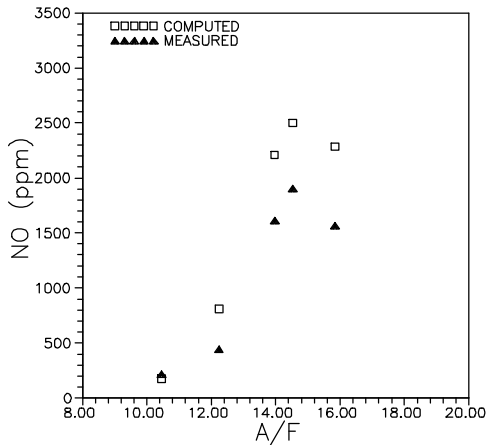


figure 10 - Comparison between computed and measured  $\text{NO}_x$  as function of Air-Fuel ratio at 3000 rpm, 90 [Nm] Torque and spark advance 15 [deg].

The HC predictions, plotted against the measured HC concentrations in the figure 11, are rather highly scattered also. The dispersion of computed data is certainly due to the influence of the unknown model parameters relating to oil layer thickness, lubricant physical characteristics, volume crevices, flame front

surface evolution and other parameters. Furthermore the cited expected overestimation is due to the neglected oxidation after the exhaust port. The computed values of HC emission as a function of air/fuel ratio for different engine operating conditions are shown in figure 12 and figure 13.

From these results, it is clear that the three emission sub-models require further improvements to reach a prediction level compatible with control applications. Moreover, the results show that the bases on which these sub-models have been built are consistent with the main physical phenomena taking place during engine cycle. Therefore, the model precision enhancement should be pursued through a more detailed description of model parameters dependencies with respect engine operating conditions. However, further physical description improvements can be still achieved for the simulation of pressure cycle (e.g. heat transfer, heat release law) and for prompt  $\text{NO}_x$  and HC exhaust port oxidation descriptions. The presented physical models have been considered as starting point for the application of the two-steps identification technique, presented in the previous section. The following model structure has been adopted:

$$y = p_1(b, n) + p_2(b, n)y_T(p(b, n)) \quad (36.)$$

Besides the parameters  $p$  included in the Taylor model  $y_T$ , further two terms  $p_1$  and  $p_2$  have been introduced. For the CO and NO models, respectively three and five physical parameters have been considered, consisting in the number of zones in the adiabatic core, in the boundary layer thickness and in the kinetic rates of the chemical reactions mainly responsible of their formation (eq. 15 for CO and Zeldovich mechanism (eq. 18) for NO)[4, 5, 16, 17]. For the HC model the following five physical parameters have been selected, consisting of the oil layer thickness, the crevices volume, the calibration constant and the kinetic rate for the post-flame oxidation reaction [18]. The maximum number of parameters  $b$  to be identified is equal to 80 for HC, to 66 for CO and to 92 for  $\text{NO}_x$  (table I). Computation of gradient and Hessian has been performed only for the components of  $p$  included in the model  $y_T$ .

Model	Number of parameters $p$ (P)	No. of physical parameters	Max No. of parameters $b$ (N)
HC	7	5	80
CO	5	3	66
$\text{NO}_x$	7	5	92

table I - Number of parameters for the three models

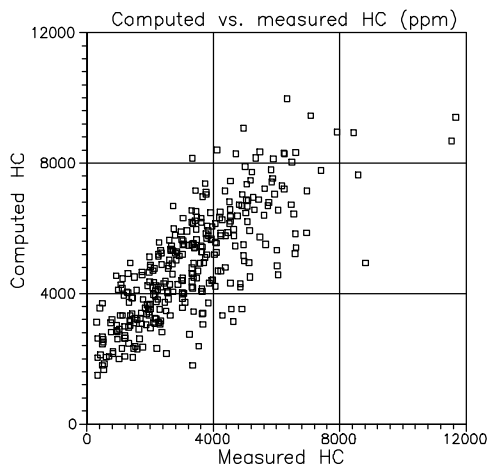


figure 11 - Computed vs. measured HC  $R^2=0.467$ .

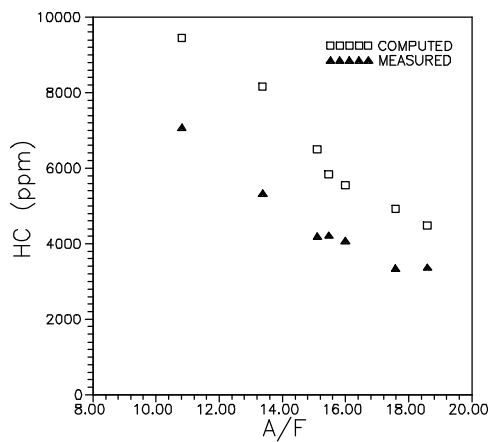


figure 12 - Comparison between computed and measured  $NO_x$  as function of Air-Fuel ratio at 1000 rpm, 30 [Nm] Torque and spark advance 35 [deg].

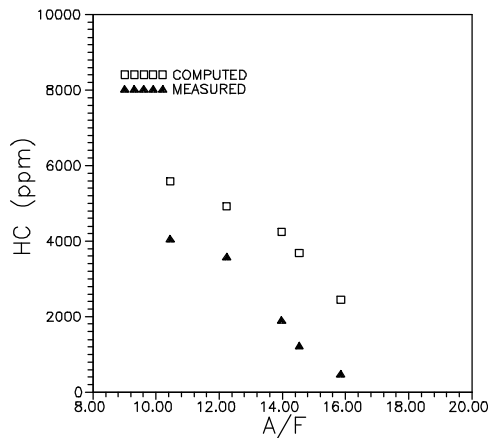


figure 13 - Comparison between computed and measured  $NO_x$  as function of Air-Fuel ratio at 3000 rpm, 90 [Nm] Torque and spark advance 15 [deg].

A vector of six engine variables  $v$  has been considered, as described in next table II:

1 - Engine speed [rpm]	4 - Engine Torque [Nm]
2 - Air/Fuel Ratio [l]	5 - Ambient Pressure [Pa]
3 - Air Flow Rate [kg/s]	6 - Spark Advance [deg]

table II- Set of engine operating variables

The ambient pressure has been used as dummy variable, to check the capability of the procedure in discarding the less significant terms. Three separate analyses have been performed for HC, CO and  $NO_x$ , because their parameters were independent.

The global results are summarized in figure 14 and table III. For each model, various solutions of the optimization problem (33, 34) are reported, for different number of parameters  $N$ . On y axis of figure 14, the relative model error is plotted (i.e. the ratio of actual value of optimal sum of squares  $S$  over the value obtained by the physical model with nominal parameters  $p_0$ ). On the abscissa, the current number of parameters  $N$  is reported. Since a backward stepwise approach has been adopted, the entire set of parameters is first included in the model, and in subsequent iterations the less significant of them are excluded. The relative error should generally be a decreasing function of  $N$ . In a first phase, where the less significant parameters are excluded, the error is almost constant. In some cases, a slight reduction of the error after the first steps may be also noticed, due to the increasing precision obtained in the subsequent numerical solutions of the problem (33, 34).

For the CO model, the relative error is almost constant passing from 66 to about 20 parameters, while it increases remarkably from 0.7 until 0.85 when only 4 parameters are used for the fitting (figure 14). It must be remarked that an improvement of the model precision is achieved even if the starting physical CO sub-model reaches a good fitting with the experimental data (figure 5, figure 15).

For the  $NO_x$  model, the relative error behavior is almost similar to the one evaluated for CO; it is constant passing from 92 to about 30 parameters, while it increases from 0.73 to about 0.78 by reducing the number of parameters from 30 to 9 (figure 14). In any cases, a significant improvement of the model precision with respect to the starting physical model is achieved (figure 8, figure 16 and table III).

For the HC model, the improvement with respect to the original model is much higher (figure 11, figure 17 and table III), being the relative error equal to about 0.40 for  $N$  ranging from 80 to 15; a relevant error reduction (about 0.45) can be still achieved even with a very small number of parameters (figure 14).

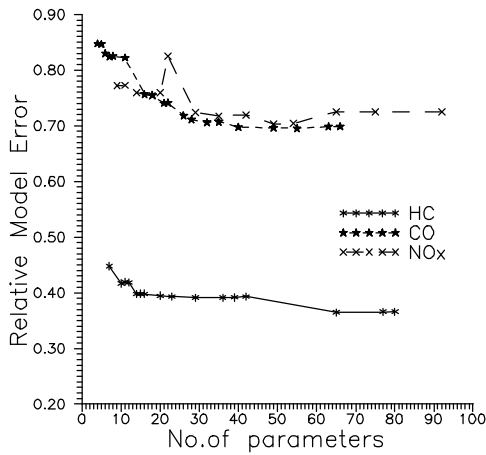


figure 14 - Relative model error vs. number of parameters for the three physical emission models

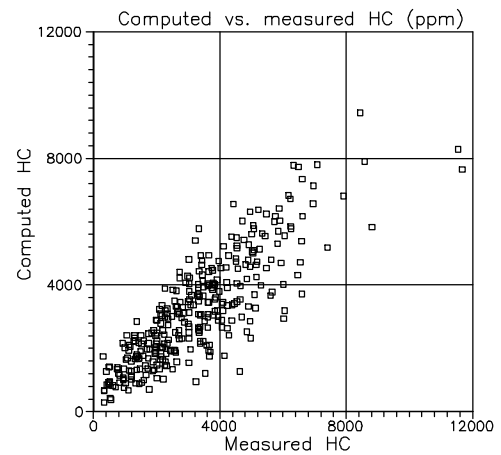


figure 17 - Measured vs. computed HC after optimization with 7 parameters  $R^2=0.708$ .

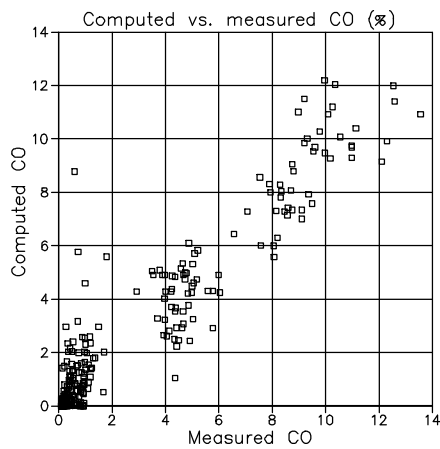


figure 15 - Measured vs. computed CO after optimization with 4 parameters  $R^2=0.897$ .

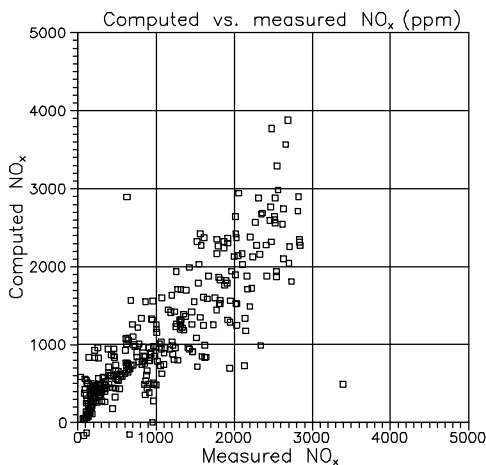


figure 16 - Measured vs. computed NO after optimization with 9 parameters  $R^2=0.531$ .

HC		CO		NO <sub>x</sub>	
<i>N</i>	<i>R</i> <sup>2</sup>	<i>N</i>	<i>R</i> <sup>2</sup>	<i>N</i>	<i>R</i> <sup>2</sup>
0	0.467	0	0.858	0	0.449
7	0.708	4	0.897	9	0.531
80	0.799	66	0.929	92	0.581
(*) 288	0.893	(*) 288	0.871	(*) 288	0.905

table III - Number of parameters and correlation index for physical and black-box(\*) models.

Further considerations have been derived from the functional form reached for the model (36). It has been found that most of the dependencies between the model parameters and the engine operating conditions are consistent with theoretical considerations on the physical phenomena governing the emission formation processes. In particular, for the HC estimation, the calibration constant  $C_R$  in eq. (23.) results to be proportional to the spark advance, expressing the indirect influence of the temperature on the post flame oxidation process. The value of the Arrhenius coefficient  $k_1$  (eq. 23.) has been found to be constant accordingly with the theory. For CO both the number of zones and the boundary layer thickness are mainly dependent on the air/fuel ratio due to its strong influence on the CO formation process, while the Arrhenius coefficient is almost constant with the engine operating conditions. In case of NO, both the boundary layer thickness and the number of zones are significantly influenced by the engine speed which relates the mixing process, modeled through the burned gases discretization, and the heat transfer between burned gases and cylinder walls.

Some cases have also been found where one or more parameters can reach values not consistent with their physical meaning. This can be avoided by imposing further constraints to the optimization problem (33, 34).

In order to quantify the increased performance obtained after the parameter optimization, a comparison of the correlation index related to the physical models ( $N=0$ ),

to the optimized models and to the black-box models is reported in table III.

Finally, the results obtained by physical models can be compared with the ones achieved, on the same data, by a black-box approach, using polynomial regression (figure 18, figure 19, figure 20 and table III).

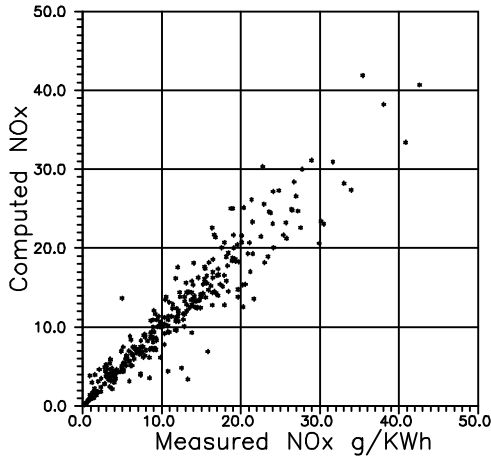


figure 18 – Black-box model - NOx

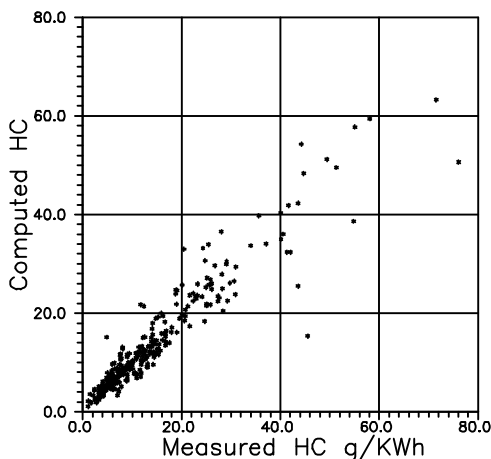


figure 19 – Black-box model - HC

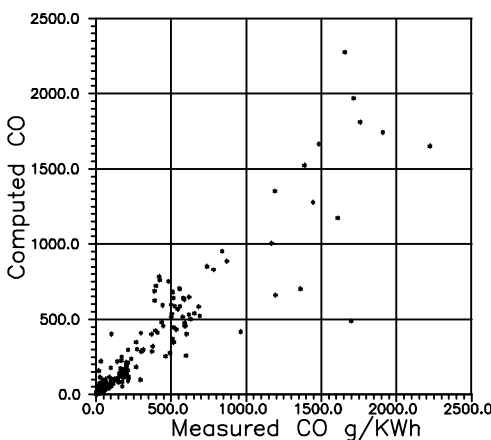


figure 20 – Black-box model - CO.

For each of the 18 points of the operating plane (Torque, rpm), a third order polynomial in two variables (air/fuel ratio and spark advance) with 16 coefficients

has been used. Thus, 288 parameters would be needed for each model. By comparing these results with the previous ones (table III), it can be observed that with the proposed modeling approach, the determination coefficient among measured and computed data reaches higher or comparable values for CO and HC, while lower precision is achieved for the NOx model. This latter, however, is influenced by a small number of outliers, presumably due to measurement errors. Therefore, this would imply that the number of experimental data for model validation can be drastically reduced, of more than one order of magnitude, by the combined use of physical models with the proposed identification technique.

The computational time required for the first step of the emission parameter optimization is strongly dependent on the number of physical parameters involved; in case of 3 physical parameters 19 iterations of the physical model are required for gradient and Hessian computation resulting in around 60 seconds for each emission estimation (HC, CO or NOx) and for each cycle, on a Pentium Pro 200 MHz. The second step is much more rapid, requiring about 30 seconds for the complete optimization over 342 cycles.

Finally, it has to be noticed that, at this stage of the work, attention has been mainly paid on development and implementation of the identification technique, rather than in the absolute precision of the physical models, outlier detection and specification of model parameters. Therefore it is reasonable to expect that further improvements could be achieved in next future by more careful analysis of such aspects.

## CONCLUSIONS

A thermodynamic model for S.I. engine cycle simulation together with three emission sub-models (CO, NO<sub>x</sub>, HC) has been presented. The whole model applications concern with engine performance simulation for control purposes and is part of a hierarchical structure of models used for the optimal design of engine control strategies.

The pressure cycle is simulated with a high level of precision over a large set of data after the identification of the burning time duration, and a physical correlation has been derived via non linear regression. From the pressure cycle calculations, emission level simulations have been performed and comparisons with a large set of experimental data have been shown.

The prediction level of emission models is in accordance with physical emissions formation mechanism, whereas further refinements are still needed in order to reach a reliable precision for predictive use. Nevertheless, the improvement of the emission sub-models can be achieved via a general identification procedure proposed by the authors, which relates sub-model parameters to engine working condition through a decomposition approach and the

iterative use of a set of regression models. The application of this technique has shown the potentiality of improving models prediction, requiring limited amount of experimental data, even starting from a not fully predictive physical model.

## ACKNOWLEDGMENTS

The authors would like to acknowledge the Engine Control Division of Magneti Marelli for the financial and technical support given to the present work.

## CONTACT

Ivan Arsie, PhD Student (*granted by European Community*).

Cesare Pianese, PhD, Contract Professor.

Gianfranco Rizzo, Associate Professor.

*Department of Mechanical Engineering, University of Salerno, 84084 Fisciano (SA), Italy*

*Ph./FAX +39 89 964069,*

*Email: grizzo@unisa.it,*

*Web page: <http://www.unisa.it>*

## REFERENCES

- [1] Hendricks E., Sorenson S.C. (1991) - *SI Engine Controls and Mean Value Engine Modelling*, SAE Paper 910258.
- [2] Gambino G., Pianese C., Rizzo G. (1994) - *Identification of a Dynamic Model for Transient Mixture Formation in a Multi-Point Spark Ignition Engine*, Proc. of Fourth ASME Symp. on Transp. System - WAM, November 6-11, 1994, Chicago, IL., DSC-vol. 54, pp 189-204.
- [3] Gambino G., Pianese C., Rizzo G. (1994) - *Experimental and Computational Analysis of a Dynamic Model for Control Strategy Optimization in a Spark Ignition Engine*, Proc. of ACC, June 29th-July 1st, 1994, Baltimore, MD, vol. 3, pp. 2374-2378.
- [4] Heywood J.B. (1988) - *Internal Combustion Engine Fundamentals*, MC Graw Hill.
- [5] Ramos J.I. (1989) - *Internal Combustion Engine Modeling*, Hemisphere Publishing Corporation..
- [6] Arsie I., Gambino M., Pianese C., Rizzo G., (1996) - *Development and Validation of Hierarchical Models for the Design of Engine Control Strategies*, Proc. of "1st Int. Conf. on Control and Diagn. in Automotive Appl.", Genova, October, 3-4, 1996, paper 96A4026, pp. 43-55, publ. on "Meccanica", Kluwer Ac.Pub., vol. 32, no. 5, pp. 397-408.
- [7] Pianese C., Rizzo G. (1996) - *Interactive Optimization of Internal Combustion Engine Tests by Means of Sequential Experimental Design*, "3rd Biennial European Joint Conference on Engineering Systems Design and Analysis - ESDA 96", Petroleum Division of ASME, Montpellier, France, July 1-4, 1996, PD-vol. 80, pp. 57-64.
- [8] Rizzo G., Pianese C. (1991) - *A Stochastic Approach for the Optimization of Open-Loop Engine Control Systems*, Annals of Operations Research n. 31, pp.545-568.
- [9] Pianese C., Rizzo G. (1992) - *A Dynamic Model for Control Strategy Optimization in Spark Ignition Engines*, Proc. Third ASME Symp. on Transp. Syst., Anaheim, CA, November 9-13, 1992, DSC 44, pp. 253-267.
- [10] Arsie I., De Franceschi F., Pianese C., Rizzo G., (1996) - *O.D.E.C.S. - A Computer Code for the Optimal Design of S.I. Engine Control Strategies*, SAE Paper 960359.
- [11] Arsie I., Di Lieto N., Pianese C., Rizzo G. (1996) - *Sviluppo e validazione di modelli termodinamici orientati ad applicazioni di controllo motore*, Proc. 51' Congr. Naz. ATI, Udine, September, 16-20, 1996, vol. 2, pp. 1449-1464 (*in Italian*).
- [12] Arsie I., Pianese C., Rizzo G. (1997) - *Identification of Emission Models for Spark Ignition Engine for Control Applications*, Proc. of 5th IIIE Mediterranean Conference on Control and Systems, Paphos - Cyprus, July, 21-23, 1997.
- [13] Ferguson C.R. (1986) - *Internal Combustion Engine*, Applied Thermosciences, Jhon Wiley.
- [14] Woschni G. (1967) - *A Universally Applicable Equation for the Instantaneous Heat Transfer Coefficient in the Internal Combustion Engine*, SAE paper 670931.
- [15] Press W.H., Flonny B.P., Teukolsky S.A. and Wetterling W.T. (1986) - *Numerical Recipes: the Art of Scientific Computing*, Cambridge Univ.Press.
- [16] Lavoie G.A., Heywood J.B., Noske G. (1970) - *Experimental and Theoretical Study of Nitric Oxide Formation in Internal Combustion Engines* - Comb.Sci. and Tech., vol. 1, pp. 313-326, 1970.
- [17] Miller J.A., Bowman C.T. (1989) - *Mechanism and Modeling of Nitrogen Chemistry in Combustion*, Progress in Energy and Combustion Science, vol. 15, n. 4, 1989.
- [18] Schramm J, Sorenson S.C. (1990) - *A Model for Hydrocarbon Emission from SI Engines*, SAE Paper 902169.
- [19] Trinker F. H., Cheng J., Davis G. C. (1993) - *A Feedgas HC Emission Model for SI Engines Including Partial Burn Effects*, SAE Paper 932705.
- [20] Lorusso J. A., Kaiser E. W. and Lavoie G. A., (1981) - *Quench Layer Contribution to Exhaust Hydrocarbons from a Spark Ignited Engine*, Combustion Science and Technologies 1981, vol. 25, pp 121-125.
- [21] Bozza F., Rizzo G. (1990) - *Un Modello di Combustione Turbolenta Multizona per MCI ad Accensione Comandata*, 45° Congresso Nazionale ATI, S. Margherita di Pula, Sept., 18-21, 1990 (*in Italian*).
- [22] Gill P.H., Murray W. & Wright M.H. (1984) - *Practical Optimization*, Academic Press, London.
- [23] Arsie I., Pianese C., Rizzo G. (1998) - *Estimation of Air-Fuel Ratio and Cylinder Wall Temperature from Pressure Cycle in S.I. Automotive Engines*, in Proc. of IFAC Workshop on "Advances in Automatic Control", Mohican State Park, Ohio, February 27 - March 2, 1998.
- [24] Arsie I, Pianese C., Rizzo G, Gambino M. (1997) *Validation of Thermodynamic Model for Spark Ignition Engines Oriented to Control Applications*, 3rd Intl. Conf. on "Internal Combustion Engines: Experiments and Modeling", Capri, September, 17-20, 1997, pp. 385-394.
- [25] Ratkowsky D.A. (1983), *Nonlinear Regression Modeling*, Dekker, New York, 1983.

## NOMENCLATURE

- $A_i$  [ ] i-th regression coefficient for combustion time duration;
- $A_b$  [m<sup>2</sup>] Combustion chamber wall area in contact with burned gases;
- $A_u$  [m<sup>2</sup>] Combustion chamber wall area in contact with unburned gases;
- $b$  [m] Cylinder bore;

$C_i$  [/] Woschni gas velocity equation constants;  
 $C_R$  [/] Calibration constant;  
 $D$  [cm<sup>2</sup>/sec] Diffusion coefficient;  
 $f$  [/] Residual mass fraction;  
 $h$  [J/kg] Specific enthalpy;  
 $h$  [W/m<sup>2</sup>/K] Convective heat transfer coefficient;  
 $k_i$  [/] i-th chemical equilibrium constant;  
 $m$  [kg] In-cylinder gas mass;  
 $m_a$  [kg] Inducted air mass per cycle;  
 $m_{cr}$  [m<sup>3</sup>] Gas mass in the crevices;  
 $rpm$  [1/min] Engine rotational speed;  
 $n$  [/] Wiebe function exponent;  
 $N$  [/] Number of parameters to be optimized;  
 $N^*$  [/] Maximum number of zones;  
 $p_i$  [/] Physical parameters coefficients;  
 $P$  [bar] In-cylinder pressure;  
 $P_{meas}$  [bar] Measured in-cylinder pressure;  
 $P_{sim}$  [bar] Simulated in-cylinder pressure;  
 $Q$  [J] Amount of heat flowing into the system;  
 $R$  [J/kg/K] Gas Constant;  
 $R^2$  [/] Correlation index;  
 $t_b$  [ms] Combustion time duration;  
 $T$  [K] Temperature;  
 $T_b$  [K] Burned gas temperature;  
 $T_p$  [K] Piston temperature;  
 $T_u$  [K] Unburned gas temperature;  
 $T_w$  [K] Cylinder wall temperature;  
 $u$  [J/kg] Specific internal energy;  
 $U$  [J] Total internal energy;  
 $v$  [m<sup>3</sup>/kg] Specific volume;  
 $V$  [m<sup>3</sup>] Total gas volume;  
 $w$  [m/s] Mean gas velocity;  
 $x$  [/] Burned mass fraction;  
 $y_{ph}$  [ppm] Output variable of the physical model;  
 $y_t$  [ppm] Taylor approximation of the physical model;  
 $Y$  [/] Fuel mass concentration in the oil layer.

$\eta_i$  [/] Engine operating variables;  
 $w$  [rad/s] Angular engine speed.

### Subscripts

$A$  Air;  
 $b$  Burned gas;  
 $cr$  Piston crevices;  
 $eq$  Chemical equilibrium conditions;  
 $EVO$  Exhaust valve opening crank angle;  
 $IVC$  Inlet valve closing crank angle;  
 $j$  Current burned gas zone;  
 $s$  Spark advance angle;  
 $u$  Unburned gas;  
 $w$  Cylinder wall.

### Greek symbols

$a$  [/] Air-Fuel ratio;  
 $b_i$  [/] parameters of the functional structure;  
 $g$  [/] Ratio of specific heats;  
 $x$  [/] Scale factor for error function;  
 $q$  [deg] Crank angle;  
 $q_b$  [deg] Angular combustion duration;  
 $q_s$  [deg] Spark advance crank angle;  
 $f$  [/] Equivalence ratio;